IEEE Photonics Journal
An IEEE Photonics Society Publication

Open Access

Channel Modeling and Characterization for Visible Light Communications

Volume 7, Number 6, December 2015

Farshad Miramirkhani
Murat Uysal

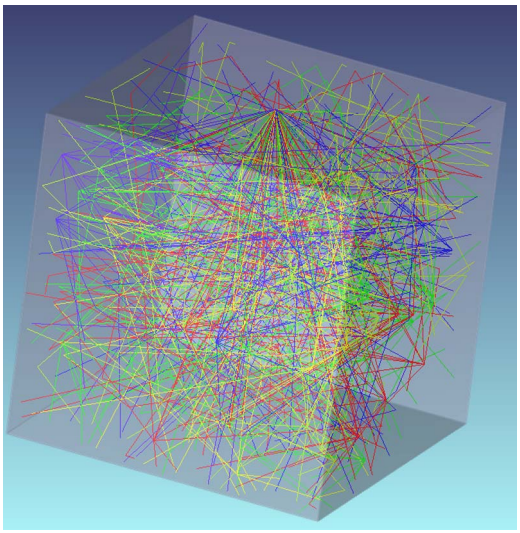

DOI: 10.1109/JPHOT.2015.2504238
1943-0655

IEEE photonics SOCIETY

IEEE

Channel Modeling and Characterization for Visible Light Communications

Farshad Miramirkhani and Murat Uysal

Department of Electrical and Electronics Engineering, Özyeğin University, 34794 Istanbul, Turkey

DOI: 10.1109/JPHOT.2015.2504238

Manuscript received September 27, 2015; revised November 24, 2015; accepted November 24, 2015. Date of publication November 26, 2015; date of current version December 8, 2015. This work was supported by the Qatar National Research Fund (a member of Qatar Foundation) under NPRP Grant 5-980-2-411. Corresponding author: F. Miramirkhani (e-mail: fmiramirkhani@yahoo.com).

Abstract: In this paper, we present a comprehensive channel modeling and characterization study for visible light communications. Our study is based on ray tracing, which allows for an accurate description of the interaction of rays emitted from the lighting source within a specified confined space. Contrary to existing works, which are mainly limited to ideal Lambertian sources and purely diffuse reflections, our approach is capable of obtaining channel impulse responses (CIRs) for any nonideal sources, as well as specular and mixed specular–diffuse reflections. Furthermore, we can precisely reflect the presence of objects (e.g., furniture) and wavelength-dependent reflection characteristics of surface materials (e.g., ceilings, floor, walls, and furniture) in a channel study. As case studies, we consider a number of indoor environments with various dimensions and different surface materials, i.e., plaster, gloss paint, wood, aluminum metal, and glass. We further consider various scenarios with different transmitter specifications (i.e., single versus multiple transmitters and array type) and receiver specifications (i.e., location and rotation). For each environment, we obtain CIRs and present a channel characterization study where channel parameters, such as channel DC gain, root mean square (RMS) delay spread, coherence bandwidth, and mean excess delay, are obtained. We also make one-to-one comparisons between infrared and visible-light CIRs for the same environments to emphasize the differences between two optical bands.

Index Terms: Visible light communications (VLC), channel modeling, ray tracing.

1. Introduction

There is an ever-increasing demand for wireless applications and services. Due to spectrum scarcity, conventional radio frequency (RF) solutions are not able to cope with this increasing demand. Low cost and highly reliable alternative and/or complementary solutions are required to enable a seamless wireless experience. Visible light communications (VLC) [1] has such a promise and depends on the dual use of the existing illumination infrastructure, i.e., light emitting diodes (LEDs) for wireless communication purposes. The human eye perceives only the average intensity when light changes fast enough; therefore, LEDs can transmit data without a noticeable effect on the lighting output and the human eyes.

There is a growing literature on VLC spanning from advanced physical layer techniques to networking, see e.g., [2]–[15] and the references therein. Despite this increasing attention on VLC systems, there is a lack of proper visible light (VL) channel models. This is a serious concern since channel modeling is the very first step for efficient, reliable, and robust VLC system

design. In the past, many works have been reported on infrared IR channel modeling [16]–[25] most of which depend on either recursive calculation methods [16]–[18] or Monte Carlo ray tracing approaches [22]–[24]. It should be however noted that there exist significant differences between VLC and IR communications and those results cannot be applied to VLC channel modeling in a straightforward manner. For example, an IR source can be approximated as a monochromatic emitter while a white light LED source is inherently wideband (380–780 nm). This calls for the inclusion of wavelength-dependency of source in VLC channel modeling. Furthermore, in IR communication, the reflectance of materials is typically modeled as a constant. On the other hand, the reflectance of materials in the VL spectrum should be taken into consideration due to the wideband nature of VLC link.

There have been some sporadic efforts [26]–[30] to address VLC channel modeling. Particularly, in [26], Monte Carlo ray tracing is used to evaluate the channel impulse response (CIR) of an empty room at VL wavelengths, but wavelength dependency is ignored considering fixed reflectance values for surface materials. In [27] and [28], recursive method proposed in [16] is used to obtain CIR in VL band, but again, fixed reflectance is assumed. In [29], in an effort to reflect the effect of wavelength dependency in channel modeling, the reflectance values are calculated as the average of wavelength dependent coefficients over the VL band.

So far, the only work which explicitly takes into account wavelength dependency is reported in [30] where a recursive method is used to determine the CIR of an empty room. However, similar to [26]–[29], the work in [30] is also limited to the assumptions of only purely diffuse reflections and ideal Lambertian source which might not hold true for many practical cases.

In this paper, we propose a realistic VLC channel modeling approach which overcomes the limitations in [26]–[30] and present several CIRs for various indoor environments based on the proposed approach. Our study is based on Zemax®; a commercial optical and illumination design software [31]. Although the main purpose of such software is optical system design, we take advantage of the ray tracing features of this software which allows an accurate description of the interaction of rays emitted from the lighting source within a specified confined space. The simulation environment is created in Zemax® and enables us to specify the geometry of the environment, the objects within, as well as the specifications of the sources (i.e., LEDs) and receivers (i.e., photodiodes). For a given number of rays and the number of reflections, the non-sequential ray tracing tool calculates the detected power and path lengths from source to detector for each ray. These are then imported to Matlab® and processed to yield the CIR. Our results demonstrate that our approach yields the same CIR as in [30] under the assumption of purely diffuse reflections and ideal Lambertian source. Our approach is further capable to obtain CIRs for any other (non-ideal) source types as well as specular and mixed specular-diffuse reflections.

As case studies, we consider a number of indoor environments with various dimensions and different surface materials, i.e., plaster, gloss paint, wood, aluminum metal, glass. We further consider various scenarios with different transmitter specifications (i.e., single vs. multiple transmitters and array type) and receiver specifications (i.e., location and rotation). For each environment, we obtain CIRs and present a channel characterization study where channel parameters such as channel DC gain, root mean square (RMS) delay spread, coherence bandwidth, and mean excess delay are obtained. We also make one-to-one comparisons between IR and VL CIRs for the same environments to emphasize the differences between two optical bands.

The remainder of the paper is organized as follows. In Section 2, we describe the methodology adopted for channel modeling. In Section 3, we consider a rectangular empty room as described in [30] and confirm the accuracy of our approach with comparison to the results presented therein. In Section 4, we present CIRs for various indoor environments with and without furniture and discuss the effect of system parameters on the CIR. We finally conclude in Section 5.

2. Methodology for Channel Modeling

Fig. 1 provides an overall summary of major steps followed in the adopted channel modeling methodology. In the first step, we create a 3-D simulation environment where we can specify

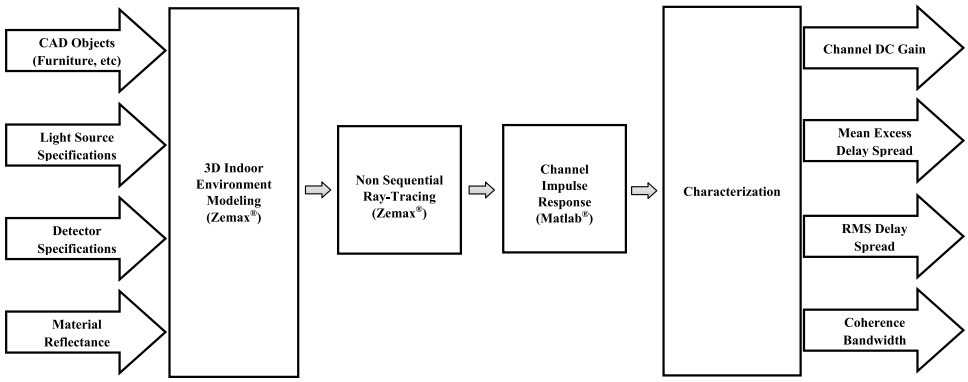

Fig. 1. Steps in channel modeling and characterization.

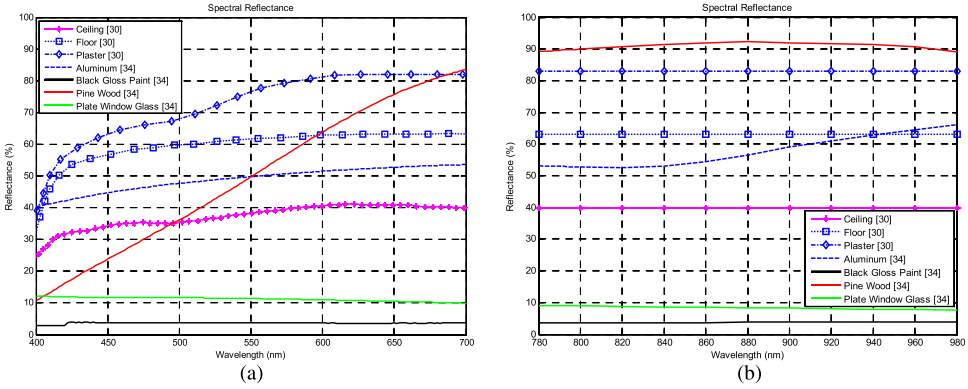

Fig. 2. Spectral reflectance of various materials (a) in the VL band and (b) in the IR band [30], [34].

the geometry of the indoor environment, the objects within, the reflection characteristics of the surface materials, and the specifications of the light sources and detectors. In the second step, we use non-sequential ray tracing feature of Zemax® to calculate the detected power and path lengths from source to detector for each ray. In the third step, we import this data to Matlab® and obtain the CIRs for the environment under consideration. Further details for each step are elaborated in the following.

2.1.1. Modeling of the Indoor Environment

To model the simulation environment, we need to specify the dimensions and shape of the indoor environment, furniture and objects within, type of surface materials (coating), as well as the properties and locations of the transmitter (LED) and receiver (photodiode). The indoor environment (i.e., office room, living room, etc) is created using Zemax® "Part Designer," which is an interface that allows to create and manipulate user-defined 3-D geometries. The CAD objects can be imported in the software to model furniture and any other objects within the indoor environment. "Table Coating Method" in the software further allows defining the wavelength-dependent reflectance of surface coating for each material [32], [33]. As noted earlier, wavelength dependency is particularly important in VL band. To emphasize the difference characteristics between IR and VL spectral bands, reflectance values for some typical materials are presented in Fig. 2. As observed, the reflectance of most materials can be safely assumed to be a constant in IR band for most practical purposes while the wavelength dependency needs to be taken into account for VL band.

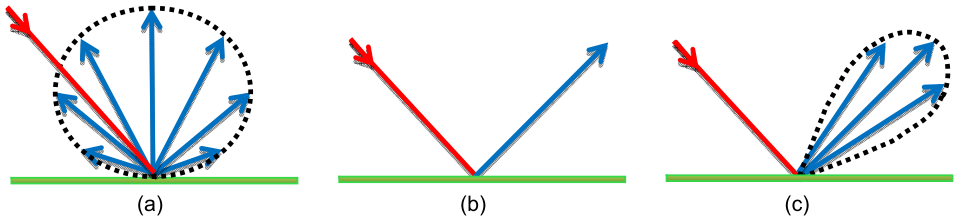

Fig. 3. (a) Purely diffuse reflections. (b) Specular reflections. (c) Mixed reflections.

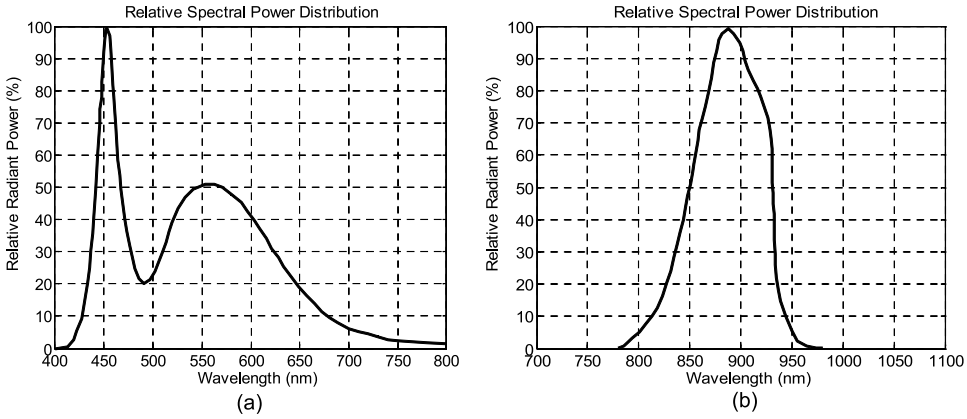

Fig. 4. Relative spectral power distribution of (a) Cree Xlamp® MC-E White LED and (b) OSRAM® SFH 4283 IR 880 nm.

Another important parameter in modeling of surface materials (walls, ceiling, furniture, etc.) is the type of reflections. As an example, Fig. 3 shows three different types where purely diffuse, specular and mixed reflections are observed. In Zemax®, we can take into account the specific type of reflection by "scatter fraction (SF)" parameter that determines the value of diffuse reflections in materials. This parameter changes between 0 and 1 such that zero indicates the purely specular reflections and unity indicates purely diffuse case.

In addition to realistic modeling of surface materials, Zemax® also allows the use of realistic light sources. Several commercially available light sources are available in Radiant Source Model (RSM) database [31]. RSM file for a light source contains the measured radiant or luminous intensity of the source as a function of wavelength, position, and angle. As such, this file can be accurately used to characterize the behavior of the light source in both near- and far-fields. As an example, Fig. 4 depicts relative power distribution of VL and IR LEDs selected from RSM database within their working wavelength range. The VL LED [see Fig. 4(a)] is a Cree Xlamp® MC-E White LED with Lambertian distribution and a viewing angle of 120° [35]. The IR LED [see Fig. 4(b)] is an OSRAM® SFH 4283 IR 880 nm LED with the same viewing angle and Lambertian distribution [36]. It can be observed from Fig. 4(b) that the full width at half maximum (FWHM) spectral bandwidth of IR LED is approximately 75 nm. On the other hand, in Fig. 4(a) shows that, unlike the IR LED, the VL LED has a large spectral bandwidth from 400–800 nm.

In Zemax®, detectors can be modeled as planar surfaces, curved surfaces or three-dimensional volumes which store the different data types such as incoherent irradiance, coherent irradiance, coherent phase, radiant intensity, radiance, and true color photometric. Moreover, the data is available in radiometric and photometric units such as watts, lumens, lux, phot, and footcandles. In our simulations, we use a rectangular surface with specified dimensions as a receiving element (i.e., "Detector Rectangle" function in Zemax®).

2.1.2 Non-Sequential Ray Tracing

After we create the simulation environment in Zemax®, we use its non-sequential ray tracing feature to determine the CIR. In ray tracing approach, rays are traced along a physically realizable path until they intercept an object. The line-of-sight (LOS) response is straightforward to obtain and depends upon the LOS distance. Besides the LOS component, there are a large number of reflections among ceiling, walls, and floor, as well as any other objects within the environment. The way that non-sequential rays are traced depends on the source properties including polarization state, coherence length, initial phase, position and direction of rays of light emanating from non-sequential sources. The random ray tracing methods used in Zemax® are mainly based on Monte Carlo analysis [37], [38] and Sobol sampling the latter of which is used for speeding up ray tracing [39], [40]. The main parameters in ray tracing are the number of rays (N_r) and the number of reflections (k). The number of reflections in Zemax® is adjusted through "Relative Minimum Intensity". For example, if this parameter is set to 10^{-5}, the software runs until the ratio of the intensity of last segment with respect to the first segment becomes 10^{-5}.

2.1.3 Determination of CIR

The non-sequential ray tracing tool generates an output file, which includes the detected power and path lengths from source to detector for each ray. We import this file to Matlab®, and using this information, we can express the CIR as

$$h(t) = \sum_{i=1}^{N_r} P_i \, \delta(t - \tau_i) \tag{1}$$

where P_i is the power of the ith ray, τ_i is the propagation time of the ith ray, $\delta(t)$ is the Dirac delta function, and N_r is the number of rays received at the detector.

2.1.4 Channel Characterization

Once we obtain CIRs, we can calculate several channel parameters such as RMS delay spread, mean excess delay, channel DC gain and coherence bandwidth. Channel DC gain (H_0) is one of the most important features of a VLC channel, as it determines the achievable signal-to-noise ratio for a fixed transmitter power and is calculated as

$$H_0 = \int_{-\infty}^{\infty} h(t)dt \tag{2}$$

The time dispersion parameters of channel, RMS delay spread and mean excess delay, are, respectively, given by [41]

$$\tau_{RMS} = \sqrt{\frac{\int_0^{\infty} (t - \tau_0)^2 h(t)dt}{\int_0^{\infty} h(t)dt}} \tag{3}$$

$$\tau_0 = \frac{\int_0^{\infty} t \times h(t)dt}{\int_0^{\infty} h(t)dt} \tag{4}$$

The frequency correlation function can be obtained from the CIR as

$$H(\Delta f) = \int_{-\infty}^{\infty} h(t) e^{-j2\pi\Delta f t} dt \tag{5}$$

For a particular correlation level c (typically chosen as 0.9, 0.7 or 0.5 [42]), coherence bandwidth (B_c) is defined as the minimum frequency separation for which the norm of the

TABLE 1
Comparison of different approaches for channel modeling

	Method	Modeling of Reflectance	Number of Reflections	Assumptions
	Proposed approach	Wavelength Dependent	High Order (10 or more reflections are possible)	- Diffuse, specular and mixed reflections - Room with furniture or any other indoor environment - Realistic measured source
[26]	Monte Carlo Ray Tracing	Fixed Reflectance	Third Order	- Purely Lambertian reflections - Empty room - Ideal Lambertian source
[27]	Recursive	Fixed Reflectance	First Order	- Purely Lambertian reflections - Empty room - Ideal Lambertian source
[28]	Recursive	Fixed Reflectance	First Order	- Purely Lambertian reflections - Empty room - Ideal Lambertian source
[29]	Recursive	Averaged Reflectance	Fourth Order	- Purely Lambertian reflections - Room with furniture - Ideal Lambertian source
[30]	Recursive	Wavelength Dependent	Third Order	- Purely Lambertian reflections - Empty room - Ideal Lambertian source

frequency correlation function across this level. It is calculated as

$$B_c = \min(\Delta f) \text{ such that } |H(\Delta f)| = c \tag{6}$$

3. Comparison With Existing Models

As discussed in Section 1, there have been only some sporadic efforts to address VLC channel modeling in the literature [26]–[30]. A comparison of underlying assumptions in the existing works and our approach is provided in Table 1.

As seen from Table 1, the only existing work which considers wavelength dependent reflectance is [30]. All the works including [30] assume only diffuse reflections and ideal Lambertian source. Furthermore, they are restricted by the number of reflections due to computation time. In contrary, our approach is more flexible and computationally less demanding. All types of reflections (i.e., diffuse, specular and mixed) can be easily taken into account. Furthermore, it is not only limited to Lambertian source and can handle all types of light sources. Since Zemax® uses "Sobol sampling" [39], [40], simulations require relatively less computing time in comparison to conventional ray tracing approaches. Therefore, it is possible to obtain CIRs based on a larger number of reflections for a better accuracy.

To make a one-to-one comparison, we consider the same environment and parameters of [30], see Fig. 5 and related parameters in Table 2. Specifically, we consider a room size of 5 m $\times$ 5 m $\times$ 3 m, where four LED luminaries are located on the ceiling, and the detector is located at the corner of the floor, as in Fig. 5. An LED luminary consists of 100 LED chips and each chip radiates 0.45 W with a view angle of 120°. The FOV and area of the detector are 85° and 1 cm^2 respectively. The reflection of materials in [30] is considered as purely diffuse and an ideal Lambertian source is used. In our case, we use Cree Xlamp® MC-E White LED [see Fig. 5(b)] which has nearly-ideal Lambertian pattern.

In Fig. 6, we present the CIR obtained through the proposed approach. The CIR of [30] is also included as a benchmark. We assume $k = 3$ reflections similar to [30]. It is observed that two CIRs are almost identical confirming the accuracy of our approach. Some small differences between the tails of two CIRs are observed. This is due to the fact that our light source is a commercial light source and not ideal Lambertian [see Fig. 5(b)] unlike the theoretical one in [30]. It can be further noted that three peaks exist in CIR which are related to four LED lightings.

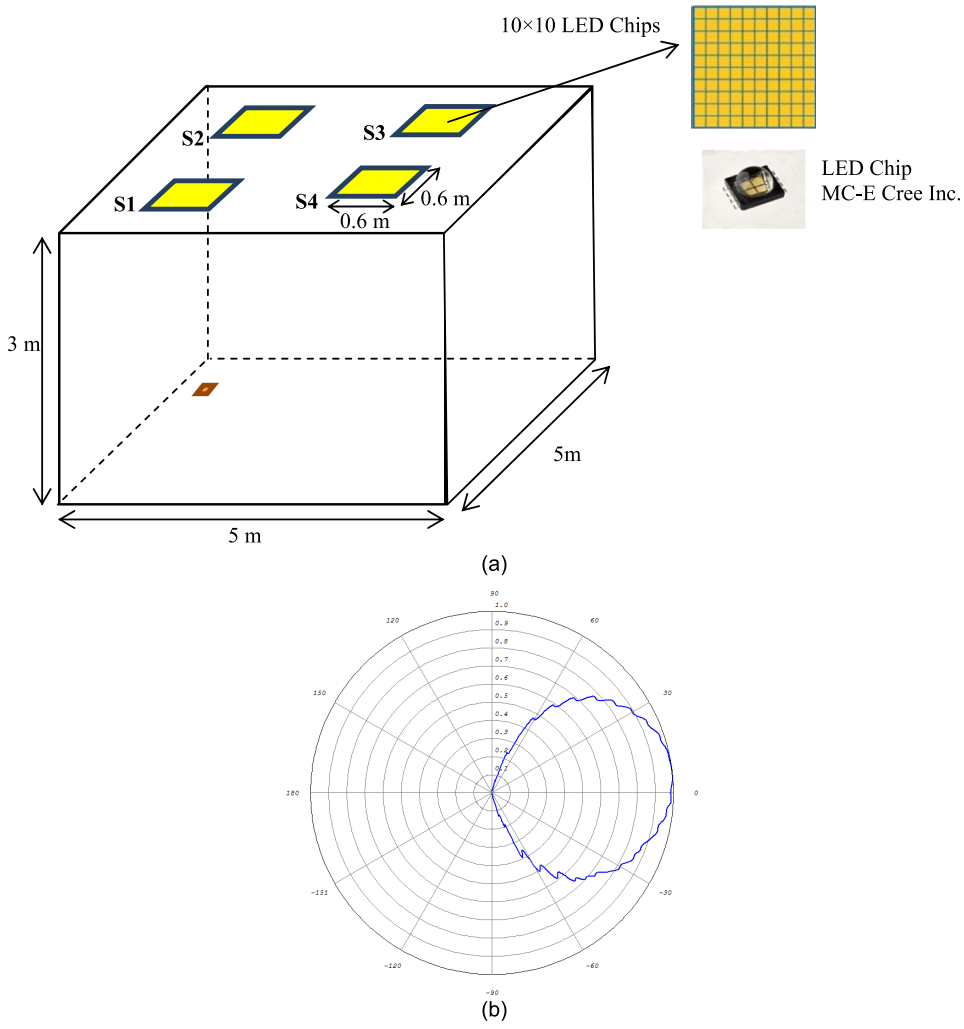

Fig. 5. (a) Three-dimensional environment. (b) Emission pattern of source.

TABLE 2

Parameters of scenario in [30]

Size of room (m)	5×5×3
Time resolution (Δt)	0.2 (ns)
Number of lighting	4
Number of chip per each lighting	100
Power of each chip	0.45 (W)
Lighting positions (m)	(1.5,1.5,3) (1.5,3.5,3) (3.5,1.5,3) (3.5,3.5,3)
PD position (m)	(0.5,1,0)
View angle of lighting	120°
FOV of PD	85°
Area of PD	1(cm^2)
Materials	Purely diffuse reflections

The largest one corresponds to the nearest LED (S2), and the second one is related to two LEDs (S1 and S3), which are at the same distance from the photodetector (PD), and the last one is related to the farther LED (S4).

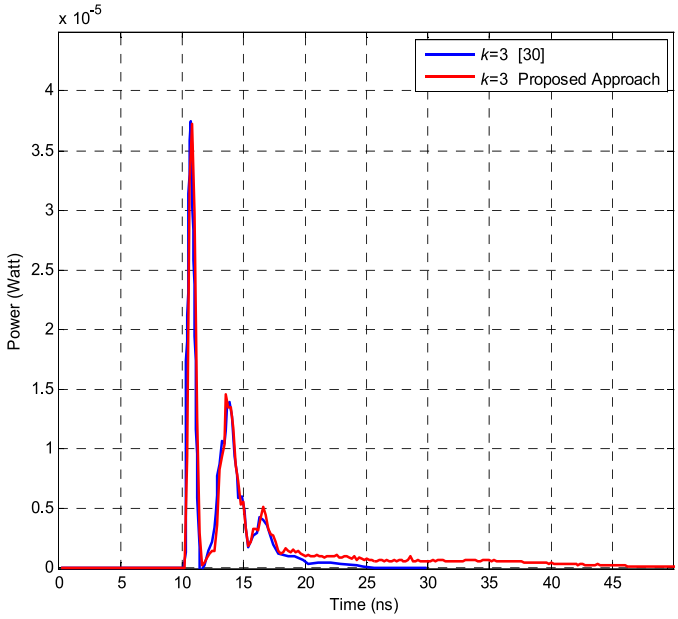

Fig. 6. Comparison of the proposed approach with [30].

TABLE 3

Mean excess delay, RMS delay spread, and channel DC gain for different k values in purely diffuse reflections

k	τ_0 (ns)	τ_{RMS} (ns)	H_0
0	12.58	2.10	4.825×10^{-5}
1	13.53	3.33	6.030×10^{-5}
2	15.59	6.60	7.068×10^{-5}
3	17.26	8.95	7.673×10^{-5}
4	17.42	9.25	7.714×10^{-5}
5	17.42	9.25	7.714×10^{-5}
6	17.42	9.26	7.714×10^{-5}
7	17.42	9.26	7.714×10^{-5}
8	17.42	9.26	7.714×10^{-5}

In Fig. 6, we assumed $k = 3$ reflections to make a one-to-one comparison with [30]; however, we note that our approach is able to handle more number of reflections. Table 3 presents mean excess delay, RMS delay spread and channel DC gain for k values up to 8. It is observed that there is no noticeable change for values larger than $k = 4$ in an empty room under consideration.

Note that the recursive approach in [30] builds upon the assumption of purely diffuse reflections. In contrary, our approach can handle other type of reflections. In the following, we assume mixed reflections (see Fig. 7) and mostly specular reflections (see Fig. 8), where SF is set to 0.5 and 0.2 respectively. It is observed from Figs. 7 and 8 that the presence of specular components create fluctuations in CIR and results in deviations from the purely diffuse case considered in [30]. This is particularly evident in Fig. 8 where mostly specular case is considered. In diffuse case, when one ray reflects from the surface, the power of ray decays by reflection coefficient and that power is divided among scattering rays. On the other hand, in the specular case, the power of ray just decays by reflection coefficient, and there is no division of power among scattering rays. By considering specular components for materials, the power of rays decays slowly which results in fluctuations of CIR.

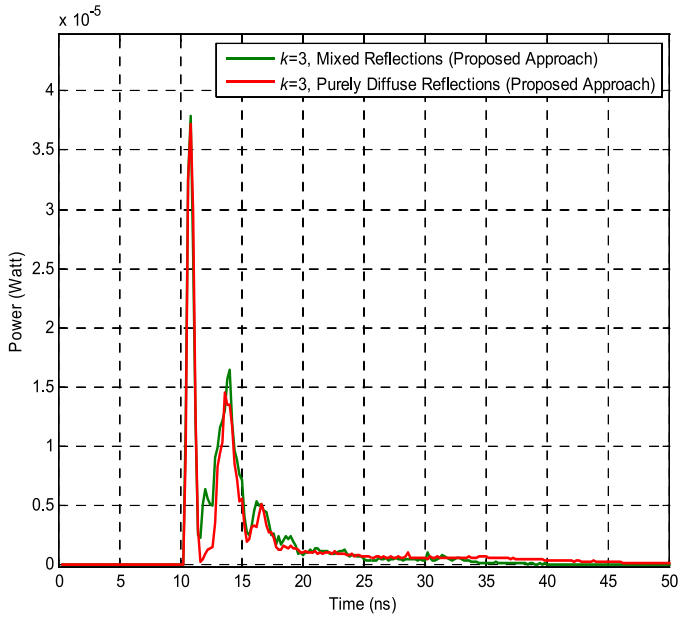

Fig. 7. Comparison of CIRs under the assumptions of mixed reflections and purely diffuse reflections.

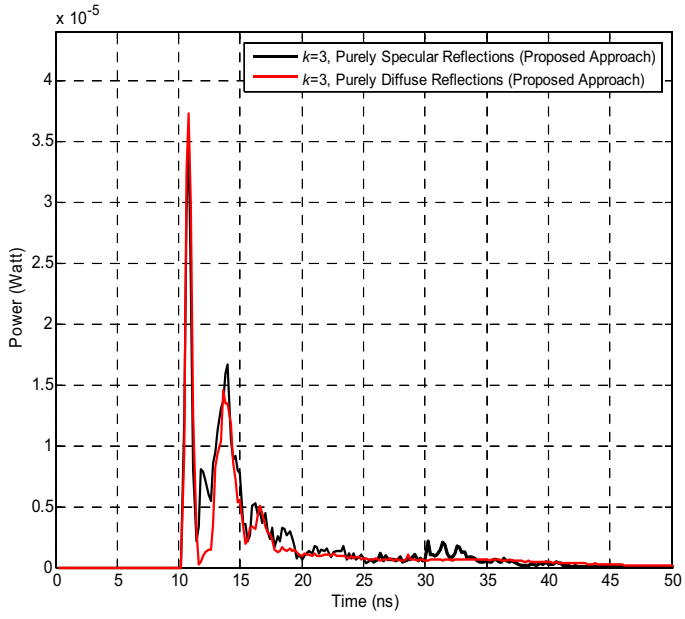

Fig. 8. Comparison of CIRs under the assumptions of mostly specular reflections and purely diffuse reflections.

To evaluate the impact of the number of the reflections on CIR, Tables 4 and 5 present the values of channel parameters for mixed and mostly specular reflection cases. It is observed that the RMS delay, mean excess delay and channel DC gain saturate after four reflections for mixed case similar to purely diffuse case. However, in the mostly specular case, this takes place after seven reflections.

TABLE 4

Mean excess delay, RMS delay spread, and channel DC gain for different k values in the case of mixed reflections

k	τ_0 (ns)	τ_{RMS} (ns)	H_0
0	12.44	1.98	4.534×10^{-5}
1	13.88	3.52	7.387×10^{-5}
2	14.76	4.93	8.063×10^{-5}
3	15.05	5.49	8.193×10^{-5}
4	15.11	5.61	8.209×10^{-5}
5	15.11	5.61	8.210×10^{-5}
6	15.11	5.61	8.210×10^{-5}

TABLE 5

Mean excess delay, RMS delay spread, and channel DC gain for different k values in the case of mostly specular reflections

k	τ_0 (ns)	τ_{RMS} (ns)	H_0
0	12.365	1.945	4.190×10^{-5}
1	13.854	3.454	7.406×10^{-5}
2	15.241	5.376	8.602×10^{-5}
3	16.469	7.124	9.198×10^{-5}
4	17.079	8.077	9.433×10^{-5}
5	17.444	8.783	9.538×10^{-5}
6	17.643	9.227	9.585×10^{-5}
7	17.744	9.491	9.605×10^{-5}
8	17.792	9.638	9.612×10^{-5}
9	17.816	9.721	9.616×10^{-5}
10	17.818	9.733	9.616×10^{-5}
11	17.821	9.744	9.616×10^{-5}
12	17.821	9.744	9.616×10^{-5}
13	17.821	9.745	9.616×10^{-5}
14	17.821	9.745	9.616×10^{-5}

4. VLC Channel Characteristics for Various Indoor Environments

In the previous section, we have introduced our channel modeling approach and compared it with some existing works highlighting our advantages. In this section, based on our approach, we present CIRs for a number of indoor environments and discuss associated channel characteristics.

4.1. Effect of Distance Between Transmitter and Receiver

In this section, we investigate the effect of varying distance between transmitter and receiver on channel parameters. We consider an empty room with a size of 10 m $\times$ 10 m $\times$ 3 m. The location of transmitter is fixed and located at the center of the ceiling. The location of receiver is varied on the diagonal which stretches from the corner to the middle of the floor. Effectively, the distance between the transmitter and receiver $(d_{\mathrm{TX-RX}})$ varies between 3 m and 7.42 m. Similar to the previous section, we assume that the FOV and area of the detector are 85° and 1 cm^2 respectively. The materials used for walls, ceiling and floor are respectively plaster, plaster and pine wood [33]. To highlight the differences between VL and IR band, we repeat the same study for IR band under the same assumptions. For VL and IR band, we use the light sources given, respectively, in Fig. 4(a) and (b).

Based on the aforementioned assumptions, Fig. 9 illustrates how channel DC gain, RMS delay spread, and coherence bandwidth change with the distance. The main observations are summarized in the following.

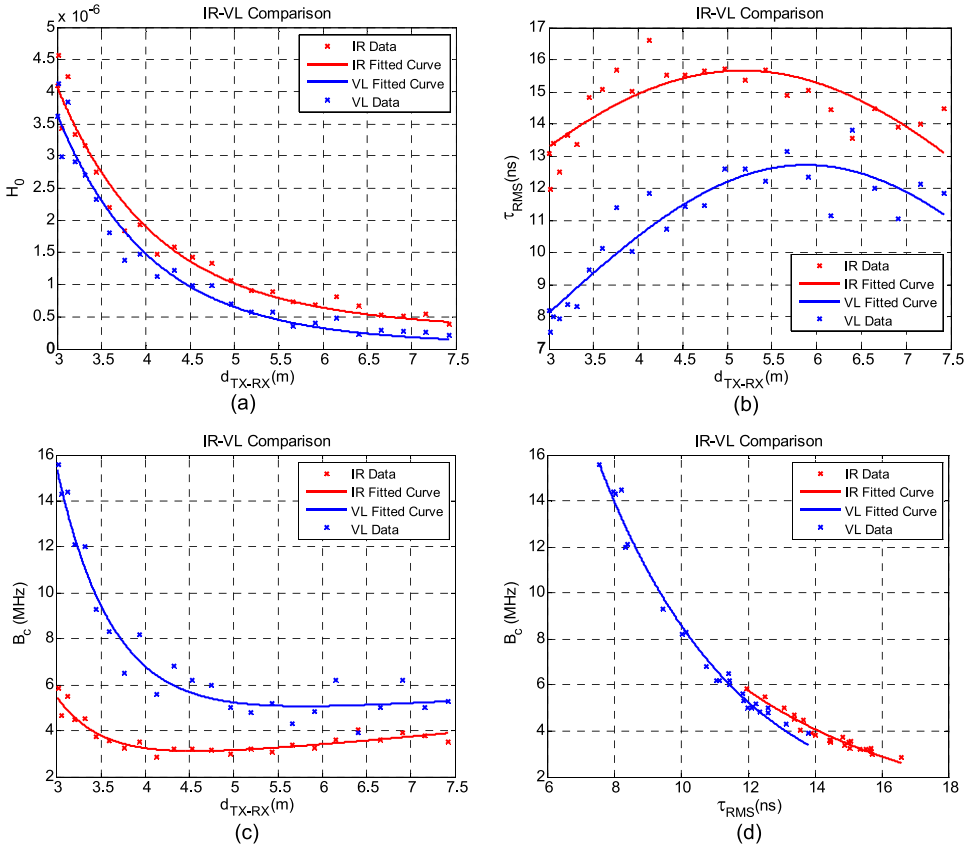

Fig. 9. (a) Channel DC gain versus distance. (b) RMS delay versus distance. (c) Coherence bandwidth versus distance. (d) Coherence bandwidth versus RMS delay spread.

4.1.1 Channel DC Gain [Fig. 9(a)]

It is observed that as $d_{\mathrm{TX-RX}}$ increases, the received power decreases in a negative exponential manner resulting in the decrease of channel DC gain. Through curve fitting, we express DC gain in terms of $d_{\mathrm{TX-RX}}$ as

$$H_0 = \begin{cases} 6.54 \times 10^{-5}\, e^{-0.99 d_{TX-RX}} + 7.52 \times 10^{-7}\, e^{-0.26 d_{TX-RX}} & \text{VL Band} \\ 5.71 \times 10^{-5}\, e^{-0.93 d_{TX-RX}} + 9.08 \times 10^{-7}\, e^{-0.12 d_{TX-RX}} & \text{IR Band} \end{cases} \tag{7}$$

Comparison of results obtained for IR and VL reveals that DC gains of VL channels are smaller than those in IR channels for same configurations. This is mainly due to the reason that reflectivity values in IR band are larger than those in VL band.

4.1.2 RMS Delay Spread [Fig. 9(b)]

It is observed that RMS delay spread first increases, then decreases with the increasing distance. It should be noted in our configuration the location of transmitter is fixed while the location of receiver is varied on the diagonal. This behavior change is a result of the detector location. Similar behavior is also reported in [43]. Through curve fitting, we express RMS delay spread in terms of $d_{\mathrm{TX-RX}}$ as

$$\tau_{RMS} = \begin{cases} 12.72\, e^{-\left(\frac{d_{TX-RX}-5.88}{4.29}\right)^2} & \text{VL Band} \\ 15.66\, e^{-\left(\frac{d_{TX-RX}-5.17}{5.34}\right)^2} & \text{IR Band} \end{cases} \tag{8}$$

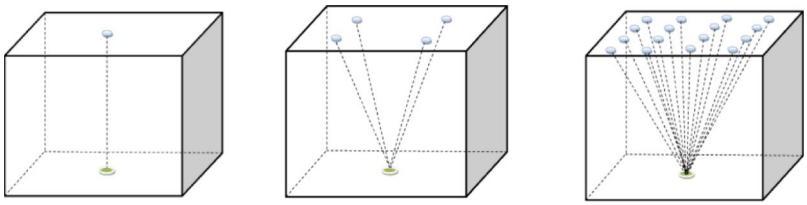

Fig. 10. Configuration with multiple light sources.

Comparison of results obtained for IR and VL reveals that RMS delay spreads of VL channels are smaller than those in IR channels for same configurations. Similar to the observations in DC gains, this happens as a result of the fact that reflectivity values in IR band are larger than those in VL band.

Our results indicate that VL channel introduces an RMS delay spread of 8–13 ns within the given environment. Targeting data speeds on the order of multiple gigabits per second will introduce inter-symbol-interference (ISI) spanning tens of symbols. This necessitates the use of proper ISI mitigation techniques for high speed VLC systems. Potential solutions such as optical orthogonal frequency division multiplexing [3], [5], [10] and equalization techniques [4], [11], [12] can be found in the VLC literature.

4.1.3 Coherence Bandwidth [Fig. 9(c) and (d)]

It is observed from Fig. 9(c) that coherence bandwidth first decreases then slightly increases with the increasing distance. This is expected as coherence bandwidth is inversely proportional to RMS delay spread. Specifically, we obtain coherence bandwidth in terms of $d_{\mathrm{TX-RX}}$ as

$$B_c = \begin{cases} 1349\ e^{-1.60 d_{TX-RX}} + 3.93\ e^{0.03 d_{TX-RX}} & \text{VL Band} \\ 896.5\ e^{-1.91 d_{TX-RX}} + 1.92\ e^{0.09 d_{TX-RX}} & \text{IR Band} \end{cases} \tag{9}$$

It is also observed from Fig. 9(c) that VL channels can potentially provide larger transmission bandwidth than IR channels.

In Fig. 9(d), we further illustrate the relation between coherence bandwidth and RMS delay spread. Through curve fitting, this relationship can be expressed as

$$B_c = \begin{cases} 1934\ \tau_{\mathrm{RMS}}^{-2.37} & 7.5 < \tau_{\mathrm{RMS}} < 14 \quad \text{VL Band} \\ 2303\ \tau_{\mathrm{RMS}}^{-2.40} & 12 < \tau_{\mathrm{RMS}} < 16.6 \quad \text{IR Band} \end{cases} \tag{10}$$

4.2 Effect of Multiple Transmitters, Position/Rotation of Transmitter/Receiver and the Presence of Objects

In the previous section, we have obtained CIRs and presented related channel parameters for an empty room with a single transmitter. In this section, we consider various environments with different transmitter specifications (i.e., multiple transmitters and array type), receiver specifications (i.e., location and rotation), and furniture.

In our study, we assume a room size of 5 m $\times$ 5 m $\times$ 3 m, where the walls and ceiling are plaster, while the floor is pinewood. The total power budget for LED chips is 1 W. Through this assumption, we associate channel DC gain with the averaged received power [16]. For easy identification, we label different configurations as VLx, x $=$ 1, 2, ... , 8 illustrated in Figs. 10–12.

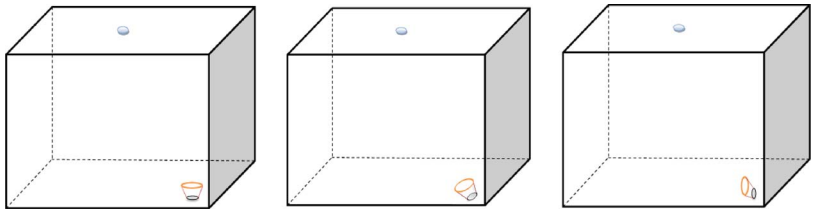

Fig. 11. Configuration with various rotations of receiver.

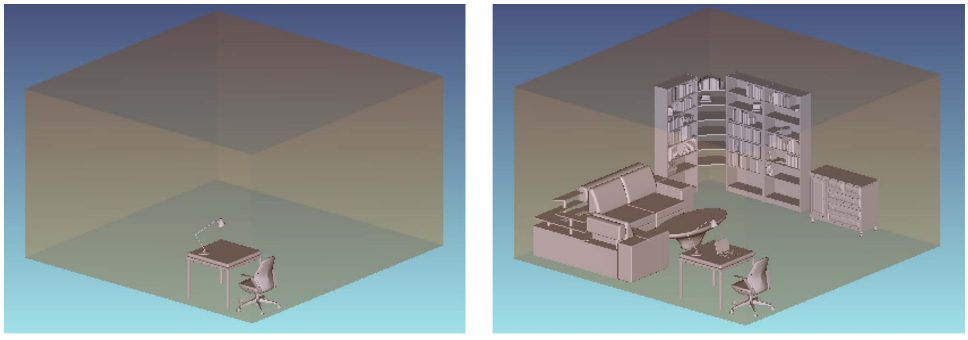

Fig. 12. Configuration with (a) few furniture and (b) lots of furniture.

TABLE 6

Channel parameters for different numbers of transmitters

Channel Parameters / Config.	τ_0 (ns)	τ_{RMS} (ns)	H_0
VL1	15.22	10.55	5.90×10^{-6}
VL2	19.92	10.60	3.02×10^{-6}
VL3	20.26	10.95	2.58×10^{-6}

4.2.1 Effect of Multi-Transmitter Deployment

In Fig. 10, we consider three configurations with different number of transmitters. The main features of these configurations are summarized below:

- **VL1:** empty rectangular room with single transmitter located at the center of the ceiling and single receiver located at the center of the floor;
- **VL2:** empty rectangular room with four transmitters located at the ceiling and single receiver located at the center of the floor;
- **VL3:** empty rectangular room with 16 transmitters located at the ceiling and single receiver located at the center of the floor.

Table 6 summarizes the channel parameters for these three configurations under consideration. It is observed that by increasing the number of transmitters (see VL2 and VL3), channel DC gain decreases with respect to VL1, where the transmitter and receiver are perfectly aligned. Note that this observation is made under the assumption of a fixed overall transmit power budget. The received power therefore decreases with LEDs more dispersed on the ceiling. It is also observed from Table 6 that RMS delay spread increases in VL2 and VL3 in comparison to VL1 with single source since more scattering is received from multiple sources.

TABLE 7

Channel parameters for different rotations of detector

Channel Parameters / Config.	T_{tr} (ns)	τ_0 (ns)	τ_{RMS} (ns)	H_0
VL4	49	26.18	11.59	1.09×10^{-6}
VL5	52	26.62	12.04	1.35×10^{-6}
VL6	51	26.34	12.97	1.17×10^{-6}

TABLE 8

Channel parameters for empty room versus furnished room

Channel Parameters / Config.	T_{tr} (ns)	τ_0 (ns)	τ_{RMS} (ns)	H_0
VL7	41	15.10	10.41	5.91×10^{-6}
VL8	37	13.08	7.80	5.58×10^{-6}

4.2.2 Effect of Position/Rotation of Receiver

In Fig. 11, we consider three configurations with different receiver rotations. The main features of these configurations are summarized below:

- **VL4:** empty rectangular room with single transmitter located at the center of the ceiling and single receiver looking upwards located at the corner of the floor;
- **VL5:** empty rectangular room with single transmitter located at the center of the ceiling and single receiver with 45 degrees rotation located at the corner of the floor;
- **VL6:** empty rectangular room with single transmitter located at the center of the ceiling and single receiver with 90 degrees rotation located at the corner of the floor.

Based on the obtained CIRs and channel parameters (see Table 7), we observe that by rotation of detector towards to the source (see VL5), the channel DC gain increases with respect to VL4 and VL6, where the receiver is pointed towards to the ceiling and walls, respectively. It is also observed that by moving the detector to the corner side, the RMS delay spread increases with respect to VL1 where the detector is located at the center of the floor. It is a result of receiving more scattering power from corner sides.

4.2.3 Effect of Objects in the Environment

In Fig. 12, we consider two different configurations to evaluate the effect of objects (e.g., furniture) in a room. The transmitter is located at the center of ceiling and the receiver is located at the center of the floor. In VL7 and VL8, we assume the same room size as VL1. The main features of these configurations are summarized below:

- **VL7:** rectangular room with chair, desk and desk lamp;
- **VL8:** rectangular room with chair, desk, desk lamp, laptop, couch, library, cage, and coffee table.

In VL7 and VL8, we assume that coating materials of desk, desk lamp, chair, cage, laptop, library, coffee table, and couch are, respectively, pinewood, black gloss paint, black gloss paint, pinewood, black gloss paint, pinewood, pinewood, and black gloss paint.

Based on the obtained CIRs and channel parameters (see Table 8), we observe that in the configuration with lots of furniture (VL8), the presence of furniture in the room has resulted in a decreased delay spread and channel DC gain. On the other hand, delay spread and channel DC gain in the room with few furniture (VL7) are similar to those ones in an empty room. It should be, however, noted that, depending on relative positions of source, detector, and furniture, different observations on CIR can made as noted in an earlier IR channel modeling study [44].

5. Conclusion

In this paper, we proposed a realistic VLC channel modeling approach based on a commercial optical and illumination design software called Zemax®. Taking advantage of the advanced ray tracing features of this software, we were able to obtain realistic CIRs which take into account practical issues such as wavelength dependency of reflection coefficients and different types of reflections (diffuse, specular and mixed cases of diffuse and specular). We were also able to integrate commercial light sources instead of ideal Lambertian sources typically used in existing works and obtain CIRs with higher order number of reflections. In the first part of the paper, to confirm the accuracy of our approach, we first demonstrated that our approach yields the same CIR as in [30] under the assumption of purely diffuse reflections and ideal Lambertian source. We then discussed the effect of specular and mixed cases. Our results demonstrated that the presence of specular components create fluctuations in CIR and result in deviations from the purely diffuse case. Furthermore, we demonstrated the importance of taking into account higher order of reflections particularly for specular cases. In the second part of the paper, we investigated the effect of varying distance between transmitter and receiver on channel parameters and obtained closed form expressions for channel DC gain and RMS delay spread as a function of distance. Our results showed that the received power decreases in a negative exponential manner resulting in the decrease of channel DC gain. It is also observed that RMS delay spread first increases then decreases with the increasing distance. Comparison of results obtained for IR and VL further reveals that DC gains and RMS delay spread of VL channels are smaller than those in IR channels for same configurations. We finally demonstrated the effect of transmitter specifications (i.e., single vs. multiple transmitters), receiver specifications (i.e., location, rotation), and objects within the environment (i.e., furniture) on the CIR.

Acknowledgment

The statements made herein are solely the responsibility of the authors.

References

[1] S. Arnon, J. R. Barry, G. K. Karagiannidis, R. Schober, and M. Uysal, Eds., *Advanced Optical Wireless Communication*, 1st ed. Cambridge, U.K.: Cambridge Univ. Press, 2012, pp. 353–368.
[2] T. Komine and M. Nakagawa, "Fundamental analysis for visible light communications using LED lights," *IEEE Trans. Consum. Electron.*, vol. 50, no. 1, pp. 100–107, Feb. 2004.
[3] R. Mesleh, H. Elgala, and H. Haas, "On the performance of different OFDM based optical wireless communication systems," *IEEE/OSA J. Opt. Commun. Netw.*, vol. 3, no. 8, pp. 620–628, Aug. 2011.
[4] K. Acolatse, Y. Bar-Ness, and S. K. Wilson, "Novel techniques of single-carrier frequency-domain equalization for optical wireless communications," *EURASIP J. Adv. Signal Process.*, vol. 2011, no. 1, Sep. 2011, Art. ID 393768.
[5] N. Fernando, Y. Hong, and E. Viterbo, "Flip-OFDM for unipolar communication systems," *IEEE Trans. Commun.*, vol. 60, no. 12, pp. 3726–3733, Dec. 2012.
[6] J. Gancarz, H. Elgala, and T. D. C. Little, "Impact of lighting requirements on VLC systems," *IEEE Commun. Mag.*, vol. 51, no. 12, pp. 34–41, Dec. 2013.
[7] A. Jovicic, J. Li, and T. Richardson, "Visible light communication: opportunities, challenges and the path to market," *IEEE Commun. Mag.*, vol. 51, no. 12, pp. 26–32, Dec. 2013.
[8] Y. Hong, J. Chen, Z. Wang, and C. Yu, "Performance of a precoding MIMO system for decentralized multiuser indoor visible light communications," *IEEE Photon. J.*, vol. 5, no. 4, Aug. 2013, Art. ID 7800211.
[9] D. Bykhovsky and S. Arnon, "Multiple access resource allocation in visible light communication systems," *J. Lightw. Technol.*, vol. 32, no. 8, pp. 1594–1600, Apr. 2014.
[10] C. W. Hsu, C. W. Chow, and C. H. Yeh, "Cost-effective direct-detection all-optical OOK-OFDM system with analysis of modulator bandwidth and driving power," *IEEE Photon. J.*, vol. 7, no. 4, Aug. 2015, Art. ID 7902607.
[11] H. Elgala and T. Little, "Polar-based OFDM and SC-FDE links toward energy-efficient Gbps transmission under IM-DD optical system constraints," *IEEE/OSA J. Opt. Commun. Netw.*, vol. 7, no. 2, pp. A-277–A-284, Feb. 2015.
[12] A. Nuwanpriya, S. Ho, J. Zhang, A. Grant, and L. Luo, "PAM-SCFDE for optical wireless communications," *J. Lightw. Technol.*, vol. 33, no. 14, pp. 2938–2949, Jul. 2015.
[13] X. Li, R. Zhang, and L. Hanzo, "Cooperative load balancing in hybrid visible light communications and Wi-Fi," *IEEE Trans. Commun.*, vol. 63, no. 4, pp. 1319–1329, Apr. 2015.
[14] G. Fekete, G. Mészáros, E. Udvary, G. Fehér, and T. Berceli, "Visible light communication channel disturbances and examination of the modulation formats," *J. Microw. Wireless Technol.*, pp. 1–9, Nov. 2015, to be published. [Online]. Available: http://journals.cambridge.org/article_S1759078715001269

[15] A. T. Hussein and J. M. Elmirghani, "Mobile multi-gigabit visible light communication system in realistic indoor environment," *Int. J. Lightw. Technol.*, vol. 33, no. 15, pp. 3293–3307, Aug. 2015.
[16] J. R. Barry, J. M. Kahn, W. J. Krause, E. A. Lee, and D. G. Messerschmitt, "Simulation of multipath impulse response for wireless optical channels," *IEEE J. Sel. Areas Commun.*, vol. 11, no. 3, pp. 367–379, Apr. 1993.
[17] F. J. Lopez-Hermandez and M. J. Betancor, "DUSTIN: Algorithm for calculation of impulse response on IR wireless indoor channels," *Electron. Lett.*, vol. 33, no. 21, pp. 1804–1806, Oct. 1997.
[18] J. B. Carruthers and P. Kannan, "Iterative site-based modeling for wireless infrared channels," *IEEE Trans. Antennas Propag.*, vol. 50, no. 5, pp. 759–765, May 2002.
[19] J. B. Carruthers and J. M. Kahn, "Modeling of nondirected wireless infrared channels," *IEEE Trans. Commun.*, vol. 45, no. 9, pp. 1260–1268, Oct. 1997.
[20] R. Perez-Jimenez, J. Berges, and M. J. Betancor, "Statistical model for the impulse response on infrared indoor diffuse channels," *Electron. Lett.*, vol. 33, no. 15, pp. 1298–1300, Jul. 1997.
[21] R. Perez-Jimenez, V. M. Melian, and M. J. Betancor, "Analysis of multipath impulse response of diffuse and quasi-diffuse optical links for IR-WLAN," in *Proc. 14th Annu. Joint Conf. IEEE Comput. Commun. Soc.*, Apr. 1995, vol. 2, pp. 924–930.
[22] F. J. Lopez-Hernandez, R. Perez-Jimeniz, and A. Santamaria, "Monte Carlo calculation of impulse response on diffuse IR wireless indoor channels," *Electron. Lett.*, vol. 34, no. 12, pp. 1260–1262, Jun. 1998.
[23] F. J. Lopez-Hernandez, R. Perez-Jimenez, and A. Santamaria, "Modified Monte Carlo scheme for high-efficiency simulation of the impulse response on diffuse IR wireless indoor channels," *Electron. Lett.*, vol. 34, no. 19, pp. 1819–1820, Sep. 1998.
[24] F. J. Lopez-Hernandez, R. Perez-Jimenez, and A. Santamaria, "Ray tracing algorithms for fast calculation of the channel impulse response on diffuse IR wireless indoor channels," *Opt. Eng.*, vol. 39, no. 10, pp. 2775–2780, Oct. 2000.
[25] M. I. Sakib Chowdhury, W. Zhang, and M. Kavehrad, "Combined deterministic and modified Monte Carlo method for calculating impulse responses of indoor optical wireless channels," *J. Lightw. Technol.*, vol. 32, no. 18, pp. 3132–3148, Sep. 15, 2014.
[26] H. Chun, C. Chiang, and D. O'Brien, "Visible light communication using OLEDs: Illumination and channel modeling," in *Proc. Int. Workshop Opt. Wireless Commun.*, Oct. 2012, pp. 1–3.
[27] H. Q. Nguyen *et al.*, "A MATLAB-Based simulation program for indoor visible light communication system," in *Proc. CSNDSP*, Jul. 2010, pp. 537–540.
[28] T. Komine and M. Nakagawa, "Performance evaluation on visible-light wireless communication system using white LED lightings," in *Proc. 9th IEEE Symp. Comput. Commun.*, 2004, vol. 1, pp. 258–263.
[29] S. Long, M. A. Khalighi, M. Wolf, S. Bourennane, and Z. Ghassemlooy, "Channel characterization for indoor visible light communications," in *Proc. IWOW*, Sep. 2014, pp. 75–79.
[30] K. Lee, H. Park, and J. R. Barry, "Indoor channel characteristics for visible light communications," *IEEE Commun. Lett.*, vol. 15, no. 2, pp. 217–219, Feb. 2011.
[31] *Zemax 13 Release 2*, Radiant Zemax LLC. [Online]. Available: www.radiantzemax.com/zemax
[32] E. Sarbazi, M. Uysal, M. Abdallah, and K. Qaraqe, "Indoor channel modeling and characterization for visible light communications," *Proc. 16th ICTON*, Graz, Austria, Jul. 2014.
[33] F. Miramirkhani, M. Uysal, and E. Panayirci, "Novel channel models for visible light communications," in *Proc. SPIE Photon. West, Broadband Access Communi. Technol. IX*, Feb. 7–12, 2015, p. 93870Q.
[34] *ASTER Spectral Library–Version 2.0*. [Online]. Available: http://speclib.jpl.nasa.gov
[35] *CREE LEDs*. [Online]. Available: http://www.cree.com
[36] *OSRAM LEDs*. [Online]. Available: http://www.osram-os.com
[37] A. Sivabalan and J. John, "Modeling and simulation of indoor optical wireless channels: a review," in *Proc. Conf. Convergent Technol. Asia-Pac. Region*, Oct. 15–17, 2003, vol. 3, pp. 1082–1085.
[38] O. Gonzalez, C. Militello, S. Rodriguez, R. Prez-Jimenez, and A. Ayala, "Error estimation of the impulse response on diffuse wireless infrared indoor channels using a Monte Carlo ray-tracing algorithm," *Proc. Inst. Elect.—Optoelectron.*, vol. 149, no. 56, pp. 222–227, Oct.–Dec. 2002.
[39] W. H. Press, S. A. Teukolsky, W. T. Vetterling, and B. P. Flannery, *Numerical Recipes*. Cambridge, U.K.: Cambridge Univ. Press, 2007.
[40] *Zemax 13 Release 2*, Radiant Zemax LLC. [Online]. Available: www.zemax.com/support/knowledgebase/understandingSobolsampling
[41] E. Sarbazi, M. Uysal, M. Abdallah, and K. Qaraqe, "Ray tracing based channel modeling for visible light communications," in *Proc. 22nd SIU Signal Process., Commun. Appl. Conf.*, Trabzon, Turkey, Apr. 2014, pp. 702–705.
[42] M. S. Varela and M. G. Sanchez, "RMS delay and coherence bandwidth measurements in indoor radio channels in the UHF band," *IEEE Trans. Veh. Technol.*, vol. 50, no. 2, pp. 515–525, Mar. 2001.
[43] Z. Ghassemlooy, D. Wu, M. A. Khalighi, and X. Tang, "Indoor non-directed optical wireless communications optimization of the Lambertian order," *J. Elect. Comput. Eng. Innov.*, vol. 1, no. 1, pp. 1–9, May 2013.
[44] M. Abtahi and H. Hashemi, "Simulation of indoor propagation channel at infrared frequencies in furnished office environments," in *Proc. IEEE PIMRC*, 1995, pp. 306–310.